Journal of Solid State Chemistry 184 (2011) 1478–1483

Contents lists available at ScienceDirect

Journal of Solid State Chemistry

journal homepage: www.elsevier.com/locate/jssc

# Magnetic ordering of divalent europium in double perovskites $Eu_2LnTaO_6$ (*Ln*=rare earths)
# Magnetic interactions of $Eu^{2+}$ ions determined by magnetic susceptibility, specific heat, and $^{151}$Eu Mössbauer spectrum measurements

Yoshitaka Misawa, Yoshihiro Doi, Yukio Hinatsu*

*Division of Chemistry, Hokkaido University, Sapporo 060-0810, Japan*

ARTICLE INFO

*Article history:*
Received 9 March 2011
Received in revised form
5 April 2011
Accepted 6 April 2011
Available online 20 April 2011

*Keywords:*
Magnetic properties
Perovskite
Europium
Magnetic susceptibility
Specific heat
Mössbauer spectrum

ABSTRACT

Structures and magnetic properties of double perovskite-type oxides $Eu_2LnTaO_6$ (*Ln*=Eu, Dy–Lu) were investigated. These compounds adopt a distorted double perovskite structure with space group $P2_1/n$. Magnetic susceptibility, specific heat, and $^{151}$Eu Mössbauer spectrum measurements show that the $Eu^{2+}$ ions at the 12-coordinate sites of the perovskite structure are antiferromagnetically ordered at ~4 K, and that $Ln^{3+}$ ions at the 6-coordinate site are in the paramagnetic state down to 1.8 K.



## 1. Introduction

It is well known that the magnetism of perovskite-type oxides $ABO_3$ is due to the *B*-site cations because the three-dimensional network of $BO_6$ octahedra gives the linear superexchange *B*–O–*B* pathway. On the other hand, the magnetic interaction between *A*-site cations is too weak, and we can seldom observe it down to 4.2 K.

It is reported that divalent europium perovskites $Eu^{2+}M^{4+}O_3$ (*M*=Ti, Zr; diamagnetic) show an antiferromagnetic ordering at 4–6 K [1,2]. In addition, when paramagnetic ions such as $Nb^{4+}$ ions are introduced at the *B*-site of the perovskites, those compounds sometimes show ferromagnetic behavior at low temperatures [3].

We focused our attention on the $Eu^{2+}$-bearing double perovskites $Eu_2LnTaO_6$. Since the trivalent *Ln* ions are located at the *B*-site of the perovskites, not only the magnetic interactions of the $Eu^{2+}$ ions at the *A*-sites, but also the interactions of the Eu–*Ln* ions are expected for $Eu_2LnTaO_6$. Previously, Sato et al. prepared a series of $Eu_2LnTaO_6$ (*Ln*=Nd–Yb, Y) compounds, and measured magnetic susceptibilities for *Ln*=Eu and Gd compounds. However, no magnetic ordering was observed down to 1.6 K [4] In this study, we performed magnetic susceptibility, specific heat, and $^{151}$Eu Mössbauer spectrum measurements for $Eu_2LnTaO_6$ (*Ln*=La–Lu). Since the total number of electrons of $Ta^{5+}$ ion is comparable to that of $Ln^{3+}$ ions, the arrangement of the *B*-site cations is not perfectly determined by the X-ray diffraction measurements. To ascertain the *B*-site cation ordering in the $Eu^{2+}$-bearing double perovskites $Eu_2LnTaO_6$, we also prepared niobium-substituted perovskite compounds $Eu_2LnNbO_6$ and measured their X-ray diffraction profiles and magnetic properties.

## 2. Experimental

### 2.1. Sample preparation

Polycrystalline samples of $Eu^{2+}$-bearing double perovskites $Eu_2LnMO_6$ (*Ln*=La–Lu; *M*=Ta, Nb) were prepared by the standard solid-state reaction. Rare earth oxides ($Ln_2O_3$, EuO), $Ta_2O_5$, Ta, $Nb_2O_5$, and Nb were used as starting materials. The EuO was prepared by heating mixtures of Eu metal (50% excess) and $Eu_2O_3$ in an evacuated quartz tube at 1073 K for 5 h and then at 1323 K for 1 h. These starting materials were well mixed in an agate mortar. The mixtures were pressed into pellets and enwrapped

* Corresponding author.
*E-mail address:* hinatsu@sci.hokudai.ac.jp (Y. Hinatsu).

0022-4596/$ - see front matter © 2011 Elsevier Inc. All rights reserved.
doi:10.1016/j.jssc.2011.04.017

with molybdenum foils, and they were sealed in evacuated silica tubes. They were fired at 1523 K for 12–24 h.

### 2.2. X-ray diffraction analysis

Powder X-ray diffraction profiles were measured using a Rigaku Multi-Flex diffractometer with Cu$K\alpha$ radiation equipped with a curved graphite monochromator. The data were collected by step-scanning in the angle range of $10^\circ \le 2\theta \le 120^\circ$ at a $2\theta$ step-size of $0.02^\circ$. The X-ray diffraction data were analyzed by the Rietveld technique, using the program RIETAN-FP [5] and the crystal structure was drawn by VESTA program [6].

### 2.3. Magnetic susceptibility measurements

The temperature-dependence of the magnetic susceptibility was measured in an applied field of 0.1 T over the temperature range of $1.8\ \mathrm{K} \le T \le 400\ \mathrm{K}$, using a SQUID magnetometer (Quantum Design, MPMS5S). The susceptibility measurements were performed under both zero-field-cooled (ZFC) and field-cooled (FC) conditions. The former was measured upon heating the sample to 400 K under the applied magnetic field of 0.1 T after zero-field cooling to 1.8 K. The latter was measured upon cooling the sample from 100 to 1.8 K in the applied field of 0.1 T.

### 2.4. Specific heat measurements

Specific heat measurements were performed using a relaxation technique by a commercial heat capacity measuring system (Quantum Design, PPMS) in the temperature range of 1.8–300 K. The sintered sample in the form of a pellet was mounted on a thin alumina plate with Apiezon grease for better thermal contact.

### 2.5. $^{151}$Eu Mössbauer spectroscopy measurements

The $^{151}$Eu Mössbauer spectra were measured with a Mössbauer spectrometer VT-6000 (Laboratory Equipment Co.) in the constant acceleration mode using a radiation source $^{151}SmF_3$ (1.85 GBq). The spectrometer was calibrated with a spectrum of $\alpha$-Fe at room temperature. The $\gamma$-rays were detected with a NaI scintillation counter. Europium trifluoride ($EuF_3$) was used as a reference standard for the chemical isomer shift. The sample was wrapped in an aluminum foil so as to have its average surface density of 10 mg (Eu) $cm^{-2}$.

## 3. Results and discussion

### 3.1. Preparation and crystal structure

The $Eu_2LnTaO_6$ compounds with $Ln$=Eu, Dy–Lu were successfully prepared, although a small amount (1–5%) of $Ln_2O_3$ was contained as an impurity phase. A representative powder X-ray diffraction profile is shown in Fig. 1(a) for $Eu_2HoTaO_6$. The results indicate that these compounds adopt the perovskite-type structure with a much lower symmetry than the cubic perovskite structure reported previously [4], and finally the observed diffraction peaks were indexed on a monoclinic cell. This unit cell is related to the primitive perovskite unit cell ($a_p$) by $a \approx \sqrt{2}a_p$, $b \approx \sqrt{2}a_p$, $c \approx 2a_p$. Fig. 2 shows the variation of lattice parameters of $Eu_2LnTaO_6$ with the ionic radius of $Ln^{3+}$ ion in the six-coordination. The lattice parameters ($a$, $b$, and $c$) increase with the ionic radius of $Ln^{3+}$ ion.

The $Eu_2LnTaO_6$ have two kinds of $B$-site cations; however, its order/disorder arrangement is not perfectly determined by the X-ray diffraction measurements because the total number of

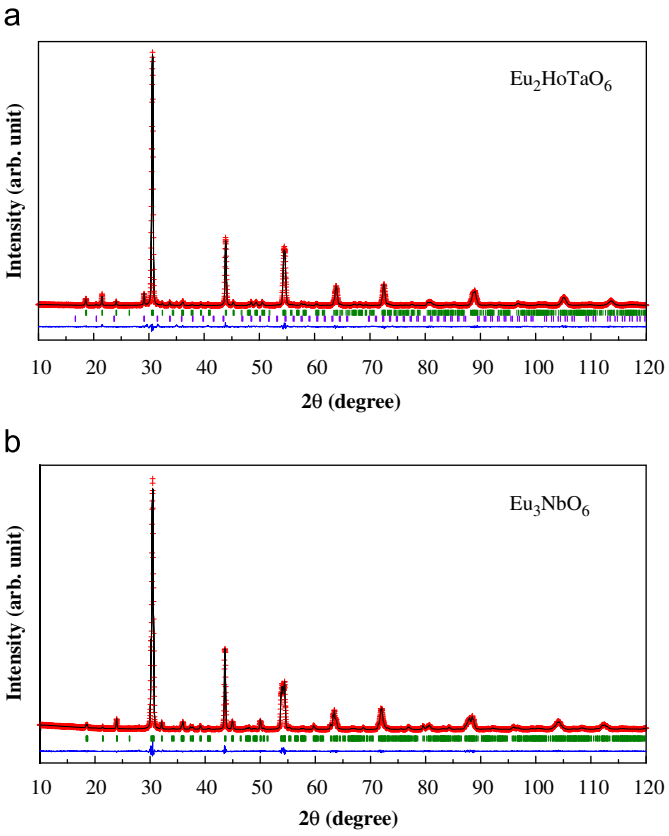


**Fig. 1.** (a) Powder X-ray diffraction profile of $Eu_2HoTaO_6$. The calculated and observed profiles are shown on the top solid line and cross markers, respectively. The first vertical marks in the middle show positions calculated for Bragg reflections. The second vertical marks show positions for an impurity of $Ho_2O_3$ (the content is 1 mol%). The lower trace is a plot of the difference between calculated and observed intensities. (b) Powder X-ray diffraction profile of $Eu_3NbO_6$.

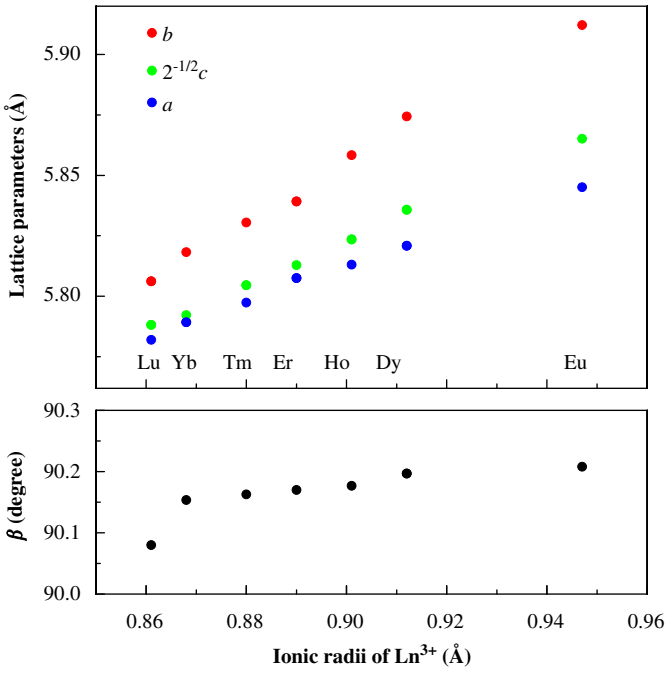


**Fig. 2.** Variation of lattice parameters for $Eu_2LnTaO_6$ with the ionic radius of $Ln^{3+}$ ion in six-coordination.

electrons of $Ta^{5+}$ ion is comparable to that of $Ln^{3+}$ ions. To ascertain the *B*-site cation ordering in the $Eu^{2+}$-bearing double perovskites $Eu_2LnTaO_6$, we prepared a europium niobate $Eu_3NbO_6$. The result of the Rietveld analysis for the X-ray diffraction measurements of this niobate is shown in Fig. 1(b). It is found that this compound has a monoclinic double-perovskite structure with space group $P2_1/n$ and Eu and Nb atoms are structurally ordered at the *B*-site with rock-salt sublattice. Structural parameters for $Eu_3NbO_7$ (atomic positional parameters and isotropic thermal parameters) are listed in Table 1. Since the ionic radius of $Ta^{5+}$ (0.64 Å) is almost the same as that of $Nb^{5+}$ (0.64 Å) [7], we have performed the Rietveld analysis of the X-ray diffraction data for $Eu_2LnTaO_6$ by assuming the same structural model as $Eu_3NbO_6$. The calculated profiles gave good fittings for all the $Eu_2LnTaO_6$ compounds. The refined lattice parameters and reliability factors for $Eu_2LnTaO_6$ are summarized in Table 2. Its crystal structure is schematically shown in Fig. 3. Table 3 lists the atomic positional parameters and isotropic thermal parameters for $Eu_2HoTaO_6$.

The average bond lengths (Eu–O, *Ln*–O and Ta–O) of $Eu_2LnTaO_6$ were calculated using the refined structural parameters. The oxidation state of the ions in these compounds is estimated by the bond valence sums (BVS) [8,9]. The BVS values for Eu, *Ln*, and Ta ions were calculated using the bond lengths, and they are listed in Table 4. The values for the *Ln* and Ta ions are almost constant (~3.3 and ~5.0, respectively) and they are reasonable for trivalent and pentavalent ions, respectively. The BVS values for the Eu ions are almost 2.0 for any of the $Eu_2LnTaO_6$ compounds, indicating that the Eu ions are in the divalent state. The following $^{151}$Eu Mössbauer spectrum measurements clearly show the oxidation state of the Eu ions in the compounds.

### 3.2. $^{151}$Eu Mössbauer spectrum

Fig. 4 shows the $^{151}$Eu Mössbauer spectra of $Eu_3TaO_6$ measured at room temperature. Two absorption peaks appeared at $\delta$=−12.3 and 1.51 mm/s, indicating that the Eu ions are in both the divalent and the trivalent states. Because of the low symmetry of the Eu sites in $Eu_3TaO_6$, the electric field gradient tensor should exist and the nonzero quadrupole interaction is expected at the Eu sites. The quadrupole Hamiltonian is given by

$$H_Q = \frac{e^2qQ}{4I(2I-1)}(3I_z^2 - I(I+1) + \eta(I_x^2 + I_y^2)) \quad (1)$$

where *I* is the nuclear spin, *Q* is the quadrupole moment, $eq = V_{zz}$, and the asymmetric parameter $\eta = (V_{xx} - V_{yy})/V_{zz}$ ($V_{ii}$ is the electric field gradient tensor). Actually, the spectra exhibited a slightly asymmetric line ($\eta \neq 0$). It is impossible to fit such a spectrum with a single Lorentzian line because of the distortion due to the quadrupole interaction. The 12 possible transitions (eight allowed transitions and four forbidden transitions) due to a quadrupole interaction were taken into account; the observed data were fitted with the sum of these Lorentzian lines (see Fig. 4). In order to derive these Lorentzian equations, the results by Shenoy and Dunlap [10] were used and the ratio of the excited and ground state quadrupole moments ($R_Q = Q_e/Q_g$) was taken as 1.312 [11]. The fitting parameters, the isomer shift ($\delta$), the quadrupole coupling constant ($eV_{zz}Q_g$) and the asymmetry parameter ($\eta$) are determined for $Eu_3TaO_6$, and they are listed in Table 5.

Fig. 5 shows the temperature dependence of the absorption area of the intensity curves of $Eu^{2+}$ and $Eu^{3+}$ ions for $Eu_3TaO_6$. At room temperature, the ratio is $Eu^{2+}$:$Eu^{3+}$=2:1. Both intensities increase monotonously with decreasing temperature, and the increase for $Eu^{2+}$ is larger than that for $Eu^{3+}$. This difference may be due to a small difference in the Debye–Waller factors between $Eu^{2+}$ and $Eu^{3+}$. The area of the intensity curve is proportional to the recoil-free fraction. Therefore, the Debye temperatures for $Eu^{2+}$ and $Eu^{3+}$ are estimated from the recoil-free fraction. The recoil-free fraction is represented by the following equation [12]:

$$f = \exp\left[\frac{-6E_R}{k\Theta_D}\left(\frac{1}{4} + \left(\frac{T}{\Theta_D}\right)^2 \int_0^{\Theta_D/T} \frac{x\,dx}{(e^x - 1)}\right)\right] \quad (2)$$

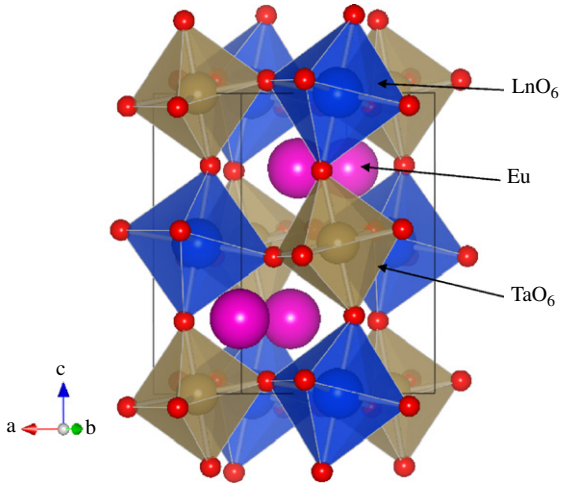


**Fig. 3.** The schematic crystal structure of $Eu_2LnTaO_6$.

**Table 1**
Structural parameters for $Eu_3NbO_6$.

| Atom | Site | *x* | *y* | *z* | *B* (Å$^2$) |
|---|---|---|---|---|---|
| Eu | 4*e* | 0.0096(3) | 0.0388(1) | 1/4 | 0.52(2) |
| Eu | 2*d* | 1/2 | 0 | 0 | 0.13(3) |
| Nb | 2*c* | 1/2 | 0 | 1/2 | 0.06(4) |
| O1 | 4*e* | −0.091(2) | 0.477(2) | 0.232(2) | 1.1(1) |
| O2 | 4*e* | 0.275(2) | 0.314(2) | 0.036(2) | 1.1 |
| O3 | 4*e* | 0.313(2) | 0.268(2) | 0.448(2) | 1.1 |

Space group: $P2_1/n$; $a$=5.8345(2) Å, $b$=5.9188(2) Å, $c$=8.2926(3) Å, $\beta$=90.280(2)°; $R_{wp}$=7.88%, $R_I$=1.59%.

**Table 2**
Lattice parameters and reliability factors for $Eu_2LnTaO_6$.

| *Ln* | *a* (Å) | *b* (Å) | *c* (Å) | $\beta$ (deg) | $R_{wp}$ (%) | $R_I$ (%) |
|---|---|---|---|---|---|---|
| Eu | 5.8451(6) | 5.9122(6) | 8.2945(8) | 90.208(4) | 10.3 | 2.54 |
| Dy | 5.8209(5) | 5.8743(4) | 8.2531(6) | 90.197(3) | 8.35 | 1.54 |
| Ho | 5.8131(4) | 5.8583(4) | 8.2357(6) | 90.177(3) | 8.70 | 1.40 |
| Er | 5.8075(2) | 5.8393(2) | 8.2207(2) | 90.170(3) | 8.00 | 2.51 |
| Tm | 5.7974(4) | 5.8305(3) | 8.2090(5) | 90.163(3) | 6.00 | 1.98 |
| Yb | 5.7893(3) | 5.8183(3) | 8.1914(4) | 90.154(3) | 7.29 | 3.82 |
| Lu | 5.7820(6) | 5.8063(8) | 8.1857(6) | 90.080(7) | 9.05 | 2.88 |

Definitions of reliability factors $R_{wp}$ and $R_I$ are given as follows: $R_{wp} = [\sum w(|F_o| - |F_c|)^2 / \sum w|F_o|^2]^{1/2}$ and $R_I = \sum |I_{ko} - I_{kc}| \sum I_{ko}$.

**Table 3**
Structural parameters for $Eu_2HoTaO_6$.

| Atom | Site | *x* | *y* | *z* | *B* (Å$^2$) |
|---|---|---|---|---|---|
| Eu | 4*e* | 0.0024(12) | −0.0295(2) | 1/4 | 0.79(3) |
| Ho | 2*d* | 1/2 | 0 | 0 | 0.28(4) |
| Ta | 2*c* | 1/2 | 0 | 1/2 | 0.10(3) |
| O1 | 4*e* | 0.069(4) | 0.525(2) | 0.234(3) | 1.0(1) |
| O2 | 4*e* | 0.272(4) | 0.302(4) | −0.042(5) | 1.0 |
| O3 | 4*e* | 0.298(4) | 0.266(4) | 0.543(5) | 1.0 |

**Table 4**
The BVS values of Eu, *Ln* and Ta ions for $Eu_2LnTaO_6$ and $Eu_3NbO_6$.

| | $Eu_3TaO_6$ | $Eu_2DyTaO_6$ | $Eu_2HoTaO_6$ | $Eu_2ErTaO_6$ | $Eu_2TmTaO_6$ | $Eu_2YbTaO_6$ | $Eu_2LuTaO_6$ | $Eu_3NbO_6$ |
|---|---|---|---|---|---|---|---|---|
| Eu | 1.86 | 1.90 | 1.89 | 1.84 | 1.91 | 1.92 | 1.95 | 1.96 |
| *Ln* | 3.37 | 2.98 | 3.38 | 3.27 | 3.31 | 3.28 | 3.20 | 3.22 |
| Ta | 5.24 | 5.18 | 5.10 | 5.40 | 5.17 | 5.15 | 5.16 | 5.00 |

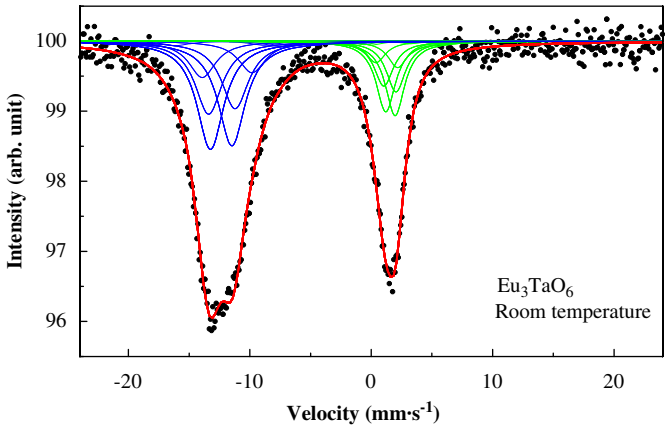


**Fig. 4.** $^{151}$Eu Mössbauer spectrum of $Eu_3TaO_6$ measured at room temperature. The red solid line is a calculated line with Lorentzians. Blue and green solid lines are 12 Lorentzians for $Eu^{2+}$ and $Eu^{3+}$ ions, respectively. (For interpretation of the references to colour in this figure legend, the reader is referred to the web version of this article.)

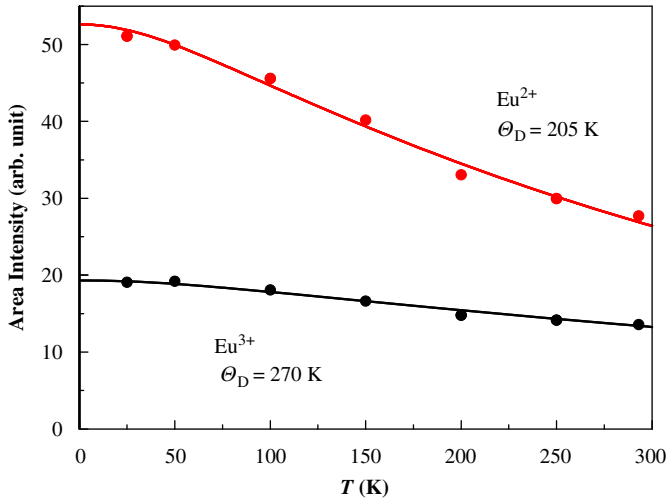


**Fig. 5.** Temperature dependence of absorption area of intensity curves (*A*) for $Eu_3TaO_6$. The red solid line is the theoretical curve of the recoil free fraction (Eq. (2), $\Theta_D$=205 K) normalized to *A* ($Eu^{2+}$) at 25 K. The black solid line is the theoretical curve of the recoil free fraction (Eq. (2), $\Theta_D$=270 K) normalized to *A* ($Eu^{3+}$) at 25 K. (For interpretation of the references to colour in this figure legend, the reader is referred to the web version of this article.)

**Table 5**
Mössbauer spectrum parameters for $Eu_3TaO_6$ at 25–300 K.

| *T* (K) | $\delta$ (mm/s) | $eV_{zz}Q_g$ (mm/s) | $\eta$ | $I_0$ (%) | $\Gamma$ (mm/s) |
|---|---|---|---|---|---|
| 300 | $Eu^{2+}$ −12.3 | 12.9 | 0.668 | 6.18 | 2.85 |
| | $Eu^{3+}$ 1.51 | 5.63 | 0.481 | 4.19 | 2.04 |
| 250 | $Eu^{2+}$ −12.2 | 13.4 | 0.815 | 5.54 | 3.70 |
| | $Eu^{3+}$ 1.55 | 9.10 | 0.971 | 3.50 | 2.78 |
| 200 | $Eu^{2+}$ −12.2 | 12.7 | 0.939 | 6.14 | 3.55 |
| | $Eu^{3+}$ 1.62 | 9.21 | 0.996 | 3.92 | 2.55 |
| 150 | $Eu^{2+}$ −12.2 | 12.8 | 0.761 | 7.61 | 3.72 |
| | $Eu^{3+}$ 1.54 | 8.88 | 0.849 | 4.47 | 2.57 |
| 100 | $Eu^{2+}$ −12.1 | 13.3 | 0.821 | 8.51 | 3.58 |
| | $Eu^{3+}$ 1.57 | 9.25 | 0.767 | 4.65 | 2.69 |
| 50 | $Eu^{2+}$ −12.1 | 13.5 | 0.741 | 11.1 | 2.99 |
| | $Eu^{3+}$ 1.59 | 5.84 | 0.822 | 5.26 | 2.41 |
| 25 | $Eu^{2+}$ −12.1 | 13.4 | 0.744 | 11.0 | 3.10 |
| | $Eu^{3+}$ 1.54 | 6.37 | 0.349 | 5.94 | 2.19 |

where *k* is the Boltzmann's constant, $\Theta_D$ is the Debye temperature, and $E_R$ is the free-atom recoil energy. By using this equation, the Debye temperatures for $Eu^{2+}$ and $Eu^{3+}$ ions are obtained to be 205 and 270 K, respectively. This result indicates that compared to the $Eu^{2+}$ ions, $Eu^{3+}$ ions are more tightly coordinated to the six oxygen ions.

The $^{151}$Eu Mössbauer spectra of $Eu_3NbO_6$ measured at room temperature are shown in Fig. 6, which is quite similar to those of $Eu_3TaO_6$. Two absorption peaks appeared at $\delta$=−12.0 and 1.56 mm/s are corresponding to the $Eu^{2+}$ and $Eu^{3+}$ ions, respectively. The absorption areas of the intensity curves of $Eu^{2+}$ and $Eu^{3+}$ ions are obtained and the ratio is $Eu^{2+}$:$Eu^{3+}$=2:1, showing that the $Eu^{2+}$ ions are located at the *A*-site of the perovskite-type structure and the $Eu^{3+}$ ions are situated at the *B*-site.

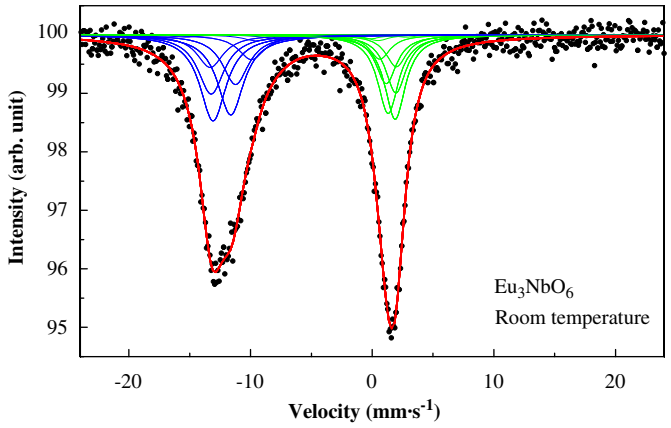


**Fig. 6.** $^{151}$Eu Mössbauer spectrum of $Eu_3NbO_6$ measured at room temperature. The red solid line is a calculated line with Lorentzians. Blue and green solid lines are 12 Lorentzians for $Eu^{2+}$ and $Eu^{3+}$ ions, respectively. (For interpretation of the references to colour in this figure legend, the reader is referred to the web version of this article.)

### 3.3. Magnetic properties

Temperature dependences of the magnetic susceptibility of $Eu_2DyTaO_6$, $Eu_2HoTaO_6$, and $Eu_2LuTaO_6$ are shown in Fig. 7(a)–(c), respectively. Any of the compounds prepared in this study showed magnetic anomaly at ca. 4 K, and no divergence between the ZFC and FC susceptibilities was observed in the whole temperature range.

The effective magnetic moments and Weiss constants determined from the Curie–Weiss law are listed in Table 6. The effective magnetic moments for $Eu_2LnTaO_6$ should be given by

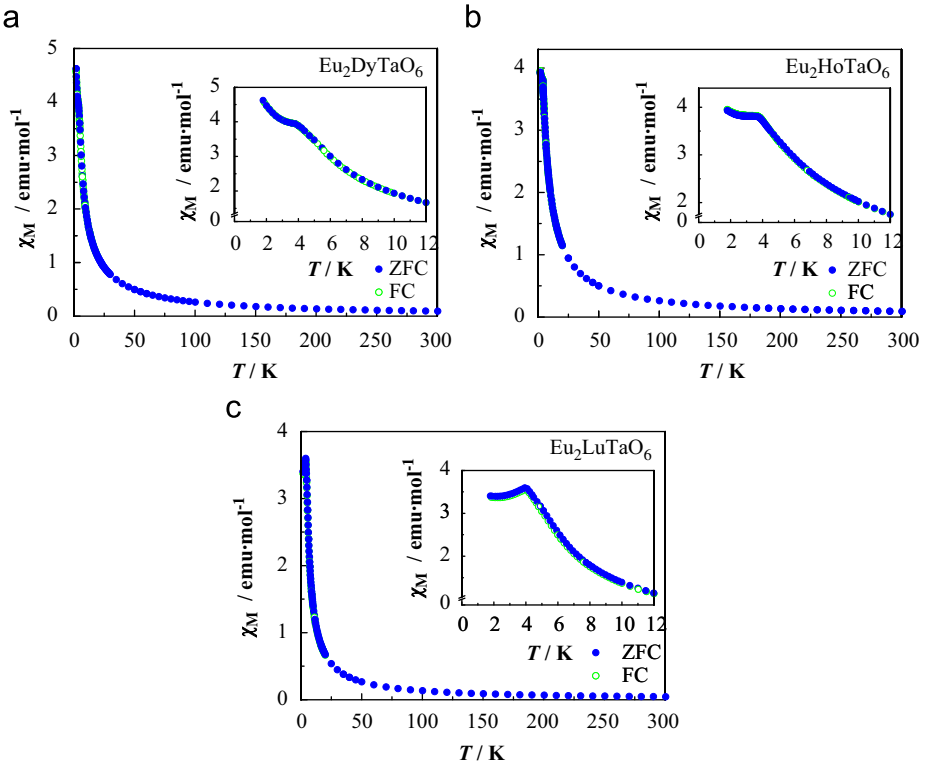


**Fig. 7.** Temperature dependences of the magnetic susceptibility of $Eu_2LnTaO_6$ ($Ln$=Dy, Ho, Lu). The insets show the susceptibility in the lower temperature region.

**Table 6**
The effective magnetic moments ($\mu_{eff}$: experimental, $\mu_{cal}$: calculated) per formula unit and Weiss constants for $Eu_2LnTaO_6$.

| *Ln* | $\mu_{eff}$ ($\mu_B$) | $\mu_{cal}$ ($\mu_B$) | $\theta$ (K) |
|---|---|---|---|
| Eu | 11.5(2) | 11.2 | −5.4(3) |
| Dy | 14.8(5) | 15.4 | −5.4(2) |
| Ho | 14.8(3) | 15.3 | −6.7(6) |
| Er | 14.3(2) | 14.6 | −5.5(4) |
| Tm | 13.2(4) | 13.3 | −10.0(2) |
| Yb | 11.4(3) | 12.0 | −4.0(2) |
| Lu | 10.5(6) | 11.2 | −1.9(2) |

the following equation:

$$\mu_{eff}^2 = 2\mu_{Eu^{2+}}^2 + \mu_{Ln^{3+}}^2 \quad (3)$$

The moments experimentally obtained are almost consistent with the moment calculated by this equation with using the free ion values of $Eu^{2+}$ and $Ln^{3+}$ ions. The Weiss constant for any compound is negative, which corresponds to the occurrence of the antiferromagnetic interactions at ca. 4 K.

To ascertain the magnetic interaction between the $Eu^{2+}$ moments, we performed the specific heat measurements in the temperature range of 1.8 and 300 K. Fig. 8(a)–(c) show the temperature dependence of the specific heat $C_p$ for $Eu_2LnTaO_6$ ($Ln$=Dy, Ho, and Lu) at low temperatures, respectively. The specific heat data show a λ-type anomaly at the temperature at which each magnetic susceptibility shows the antiferromagnetic behavior. To calculate the magnetic contribution to the specific heat ($C_{mag}$), we have to subtract the contribution of lattice specific heat ($C_{lattice}$) from the total specific heat ($C_p$), i.e., $C_{mag}=C_p-C_{lattice}$. For $Eu_2LuTaO_6$, the lattice specific heat was estimated by using a polynomial function of the temperature, $f(T)=aT^3+bT^5+cT^7$ [13] (see Fig. 8(c)), in which the constants $a$, $b$ and $c$ were determined by fitting this function to the observed specific heat data above 30 K. A dashed line in the $C_p$–$T$ curve below 1.8 K represents the extrapolated specific heat by the relation $C_p \propto T^3$ from the spin-wave model for an antiferromagnet [14]. For the lattice specific heat of $Eu_2DyTaO_6$ and $Eu_2HoTaO_6$ compounds, the data of $Eu_2LuTaO_6$ (the above-mentioned fitting results) were used. From the temperature dependence of the magnetic specific heat ($C_{mag}$), the magnetic entropy change of $Eu_2LnTaO_6$ is calculated by the relation $S_{mag}=\int(C_{mag}/T)dT$. It is shown in Fig. 9. The magnetic entropy change due to the antiferromagnetic ordering is about 30 J mol$^{-1}$ K$^{-1}$ for any of the $Eu_2LnTaO_6$ compounds. Magnetic entropy change due to the magnetic ordering of $Eu^{2+}$ ions is expected to be $R\ln(2S+1)=R\ln 8=34.5$ J mol$^{-1}$ K$^{-1}$, where $R$ and $S$ are the molar gas constant and the total spin quantum number, respectively. Although the magnetic entropy change experimentally observed is a little smaller than the theoretically expected value, this result clearly indicates that the magnetic ordering observed at 4–5 K is due to the magnetic interactions between $Eu^{2+}$ ions at the $A$-site, and that the $Ln^{3+}$ ions do not contribute to it. We consider that the difference in the magnetic entropy values found for $Ln$=Ho and Lu compounds is not due to the magnetic contribution of $Ho^{3+}$ ions to the magnetic ordering, but due to poor estimation of the lattice specific heat for the Ho compound (see Fig. 8(b)).

Magnetic ions in the $Eu_2LuTaO_6$ are only $Eu^{2+}$. This compound shows a simple antiferromagnetic behavior, i.e., its magnetic susceptibility decreases with decreasing temperature below the antiferromagnetic temperature (Fig. 7(c)). On the other hand, for the $Eu_2LnTaO_6$ compounds with paramagnetic $Ln$ ions, their magnetic susceptibilities increase with decreasing temperature below the ordering temperature (Fig. 7(a) and (b)). The magnetic ordering temperature of $Eu_2LnTaO_6$ does not change with $Ln$, and the temperature dependence of the magnetic entropy does not change between paramagnetic $Ln$ ions and diamagnetic $Ln$ ions (Fig. 9). These experimental results indicate that $Ln^{3+}$ ions at the

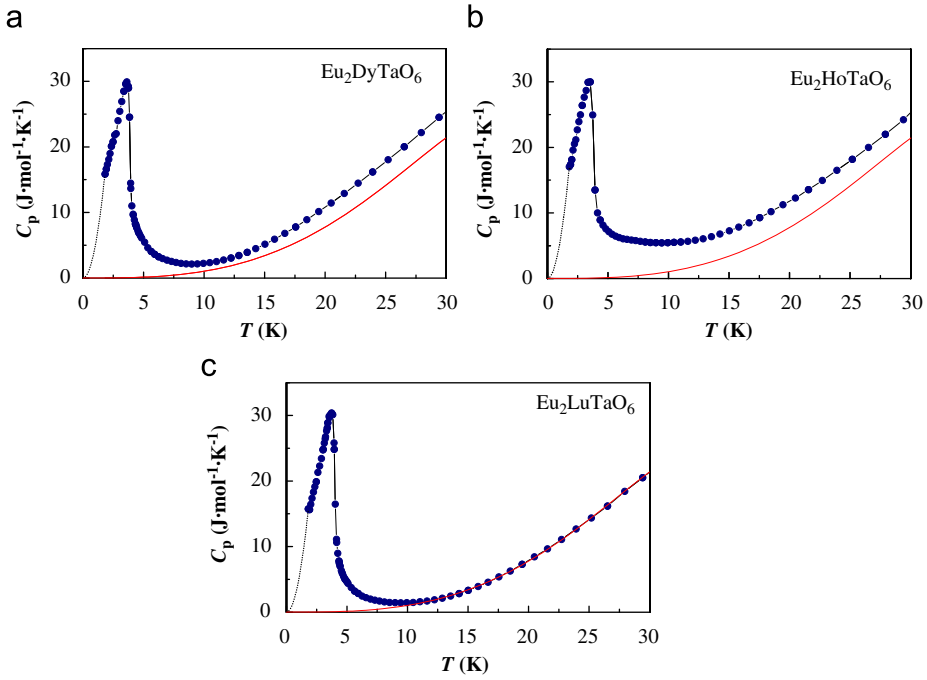


**Fig. 8.** Temperature dependence of the specific heat $C_p$ for $Eu_2LnTaO_6$ ($Ln$=Dy, Ho, Lu) at low temperatures ($T \leq 30$ K). A red solid line is the lattice specific heat calculated from fitting (see text). A dashed line below 1.8 K represents the extrapolated specific heat. (For interpretation of the references to colour in this figure legend, the reader is referred to the web version of this article.)

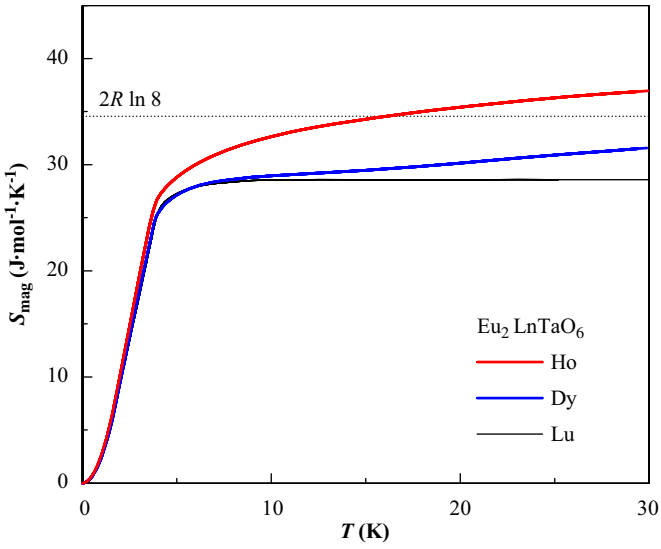


**Fig. 9.** The magnetic entropy change $S_{mag}$ for $Eu_2LnTaO_6$ ($Ln$=Dy, Ho, Lu) in the low temperature range ($T \leq 30$ K).

*B*-sites are in the paramagnetic state and that long-range magnetic ordering is due to the magnetic interactions between $Eu^{2+}$ ions at the *A*-sites.

## Acknowledgments

This work was supported by Grant-in-aid for Scientific Research, no. 20550052 from the Ministry of Education, Science, Sports, and Culture of Japan.

## References

[1] T.R. McGuire, M.W. Shafer, R.J. Joenk, H.A. Alperin, S.J. Pickart, J. Appl. Phys. 37 (1966) 981–982.
[2] Y. Zong, K. Fujita, H. Akamatsu, S. Murai, K. Tanaka, J. Solid State Chem. 183 (2010) 168–172.
[3] V.G. Zubkov, A.P. Tyutyunnik, V.A. Pereliaev, G.P. Shveikin, J. Koher, R.K. Kremer, A. Simon, G. Svensson, J. Alloys Compd. 226 (1995) 24–30.
[4] K. Sato, G. Adachi, J. Shiokawa, J. Inorg. Nucl. Chem. 38 (1976) 1287–1289.
[5] F. Izumi, K. Momma, Solid State Phenom. 130 (2007) 15–20.
[6] K. Momma, F. Izumi, J. Appl. Crystallogr. 41 (2008) 653–658.
[7] R.D. Shannon, Acta Crystallogr. A32 (1976) 751–767.
[8] I.D. Brown, A. Altermatt, Acta Crystallogr. Sect. B 41 (1985) 244–247.
[9] N.E. Brese, M. O'Keeffe, Acta Crystallogr. Sect. B 47 (1991) 192–197.
[10] G.K. Shenoy, B.D. Dunlap, Nucl. Instrum. Methods 71 (1969) 285.
[11] J.G. Stevens, in: J.W. Robinson (Ed.), Handbook of Spectroscopy, vol. III, CRC Press, Boca Raton, FL, 1981, p. 464.
[12] K. Mahesh, Phys. Status Solidi b 61 (1974) 695–700.
[13] J.E. Gordon, R.A. Fisher, Y.X. Jia, N.E. Phillips, S.F. Reklis, D.A. Wright, A. Zettl, Phys. Rev. B 59 (1999) 127–130.
[14] J. Van Kranendonk, J.H. Van Vleck, Rev. Mod. Phys. 30 (1958) 1–23.